



Effects of La substitution on microstructure and hydrogen storage properties of Ti–Fe–Mn-based alloy prepared through melt spinning

Ze-ming YUAN^{1,2}, Zhen QI^{1,2}, Ting-ting ZHAI¹, Hong-zhang WANG¹, Hai-yan WANG¹, Yang-huan ZHANG^{1,2}

1. Instrumental Analysis Center, Inner Mongolia University of Science and Technology, Baotou 014010, China;
2. Department of Functional Material Research, Central Iron and Steel Research Institute, Beijing 100081, China

Received 28 November 2020; accepted 12 July 2021

Abstract: The as-spun $Ti_{1-x}La_xFe_{0.8}Mn_{0.2}$ ($x=0, 0.01, 0.03, 0.06, 0.09$, molar fraction) alloys were prepared by melt spinning. The effects of La substitution for Ti on the microstructure, hydrogen storage kinetics and thermodynamics of TiFe-type Ti–Fe–Mn-based alloy were investigated. The as-spun alloys hold the TiFe single phase, which transforms to $TiFeH_{0.06}$, TiFeH, and $TiFeH_2$ hydrides after hydrogenation. La substitution promotes the formation of micro-defects (such as dislocations and grain boundaries) in the alloys, thus facilitating hydrogen diffusion. In addition, the hydrogen storage kinetics properties are improved after introducing La element. With the rise of La content, the hydrogen storage capacity decreases firstly and then increases, but the absolute value of hydriding enthalpy change ($|\Delta H|$) increases firstly and then reduces. When $x=0.01$, the maximum value of $|\Delta H|$ is obtained to be (25.23 ± 0.50) kJ/mol for hydriding, and the alloy has the maximum hydrogen absorption capacity of (1.80 ± 0.04) wt.% under the conditions of 323 K and 3 MPa.
Key words: La substitution; Ti–Fe–Mn-based alloy; melt spinning; hydrogen storage kinetics; thermodynamics

1 Introduction

The use of fossil energy has caused serious environmental problems and ecological crises, such as acid rain, greenhouse effect, and heat island effect. Therefore, finding a clean and efficient new energy that can replace traditional fossil energy has become one of the most important strategic measures worldwide to deal with energy and environmental issues and promote sustainable economic development [1]. Hydrogen energy is a clean, green, and sustainable energy all the time. As a new energy system that is environment-friendly, hydrogen energy can be a replacement for fossil energy and used as onboard vehicle power [2]. However, hydrogen storage is the key concern in the practical application of hydrogen energy. High-pressure compressed hydrogen storage is the traditional method but it is accompanied by many

safety hazards. Metal hydrides are safe and efficient materials for hydrogen storage and can realize the reversible absorption/desorption of hydrogen under moderate temperature and pressure [3–6]. TiFe-based alloy is a potential hydrogen storage material due to its high hydrogen storage capacity, favorable dehydrogenation temperature, moderate dehydrogenation pressure, and low cost [7–12]. However, the poor activation performance (activation for hydrogenation is required at 630 K) of TiFe-based alloy is a huge obstacle for its application [13–15]. If the Ti content in the TiFe alloy is insufficient, the $TiFe_2$ phase will coexist with the matrix phase of TiFe. Given that $TiFe_2$ does not react with hydrogen, the hydrogen absorption capacity of the alloy decreases. If the content of Ti is excessive, the reaction between Ti and hydrogen will produce TiH_2 , which is tough to decompose at low temperature. In addition, the maximum hydrogen absorption capacity of the

alloy is reduced when the excessive titanium is added. Therefore, the preparation of TiFe alloy should be optimized to ensure the use of suitable stoichiometric ratio.

Many techniques including element substitution, mechanical alloying, surface modification, and high pressure torsion, have been developed to improve the activation performance [16–25]. One of the most effective methods is element substitution. For instance, Mn substitution facilitates the activation because of the preferential oxidation of Mn and the related surface segregation. Substituting Fe with Mn affects the activation performance and reduces the activation temperature from 573 to 423 K [26]. The use of Ni part substitution for Fe can substantially improve the activation performance, and decrease the activation temperature of TiFe alloy from 573 to 443 K [27]. Titanium replacement by magnesium can also enhance the hydrogen storage performance and hydrogen charging capacity [28]. Rare earth elements, such as Ce, have been added to TiFe_{0.9}Mn_{0.1} alloy to improve the activation property and the obtained alloys can immediately absorb hydrogen at the hydrogen pressure of 4.0 MPa and the temperature of 353 K without any pretreatment [29]. Mn replacement can also enhance the activation property and reduce the incubation time to a certain extent. The above-mentioned improvements are related to the increased number of interfaces between the second phase and the TiFe main phase, and the composition of the second phase. Excellent activation performance for the alloy can be obtained by introducing a high amount of interfaces and the high activity of the second phase.

Inducing formation of nanostructures is also an effective strategy to enhance the hydrogen storage performance of TiFe-based alloy. When the grain size of TiFe-based alloy is maintained at the nanometer level, it can be fully activated and absorb hydrogen under 1 MPa hydrogen pressure [30]. Short-time ball milling is an effective process to enlarge the specific surface area and reduce the particle and grain size without changing the alloy composition [31]. Melt spinning is also a preparation method for nano-materials. The substitution of a small amount of La can remarkably enhance the activation performance of TiFe alloy [32]. In consideration of the positive

role of element substitution and melt spinning in hydrogen storage performance, in this work, Ti_{1-x}La_xFe_{0.8}Mn_{0.2} ($x=0, 0.01, 0.03, 0.06, 0.09$) alloys were prepared through melt spinning, and the microstructure and hydrogen storage properties of these alloys were also studied.

2 Experimental

The as-cast Ti_{1-x}La_xFe_{0.8}Mn_{0.2} ($x=0, 0.01, 0.03, 0.06, 0.09$, molar fraction) alloys were prepared through vacuum-induced melting in Ar atmosphere. The purity of the metals (Ti, La, Fe, Mn) was >99.7%. In consideration of the evaporative loss during the preparation, a slightly excessive (5 wt.%) La was added. Partial as-cast alloys were re-melted in a vacuum induction furnace to prepare the as-spun specimens through single roller rapid quenching. The re-melted alloys were sprayed on the surface of the rotating roller. Given that the cooling rate is difficult to measure precisely, the spinning speed was defined as the copper roller linear velocity. The spinning rate was set to be 10 m/s. The actual La amount of the as-spun alloy was measured by inductively coupled plasma (ICP), which revealed that the composition of the alloy conforms to the designed atomic ratio. For convenience, the as-spun Ti_{1-x}La_xFe_{0.8}Mn_{0.2} alloys with $x=0, 0.01, 0.03, 0.06$, and 0.09 were defined as La0, La1, La3, La6, and La9, respectively.

The samples before and after hydrogenation were characterized by X-ray diffraction (XRD) and high resolution transmission electron microscopy (HRTEM). The hydrogen storage properties were measured by a Sieverts-type apparatus. The alloys were activated under the initial pressure of 3 MPa at 423 K. Pressure composition isotherms (PCI) were measured at temperatures of 303, 323, 343 and 363 K. The accuracy of the experiment was evaluated, and the verifying experiments showed that the measurement error is less than 0.2% according to the physical factors, including pressure (precision is 100 Pa), temperature (precision is 0.01 K), time (precision is 0.01 s), and mass (precision is 0.001 g).

3 Results and discussion

3.1 Structural characterization

Figure 1 shows the XRD patterns of the

as-spun $\text{Ti}_{1-x}\text{La}_x\text{Fe}_{0.8}\text{Mn}_{0.2}$ ($x=0, 0.01, 0.03, 0.06, 0.09$) alloys before and after hydrogenation. All as-spun alloys are composed of TiFe single phase. La substitution does not change the phase composition. Figure 1(b) shows the XRD patterns of the as-spun alloys after hydrogenation at 3 MPa and 423 K. The diffraction peak expands with the increase in La substitution, indicating that this process leads to nanocrystallization. The diffraction peaks of $\text{TiFeH}_{0.06}$, TiFeH, and TiFeH_2 phases are found in the La0, La1, and La3 alloys, respectively. When the added La content is increased to 0.06, $\text{TiFeH}_{0.06}$ and TiFeH phases are observed. In

addition, a TiH phase appears when the La content is increased to 0.09. A two-step reaction, $\text{TiFe} \rightarrow \text{TiFeH} \rightarrow \text{TiFeH}_2$, occurs in the hydrogenation of TiFe alloy [33]. However, the step of TiFeH to TiFeH_2 is hindered when the La content is increased to 0.06 according to the XRD results.

The microscopic crystal structures of as-spun alloys before and after hydrogenation with La0 and La1 alloys as representatives are observed and characterized by HRTEM, as shown in Fig. 2. Similar to the results of XRD analysis, TiFe phase is observed in La0 and La1 alloys before hydrogenation (Figs. 2(a) and (c)), and TiFeH and

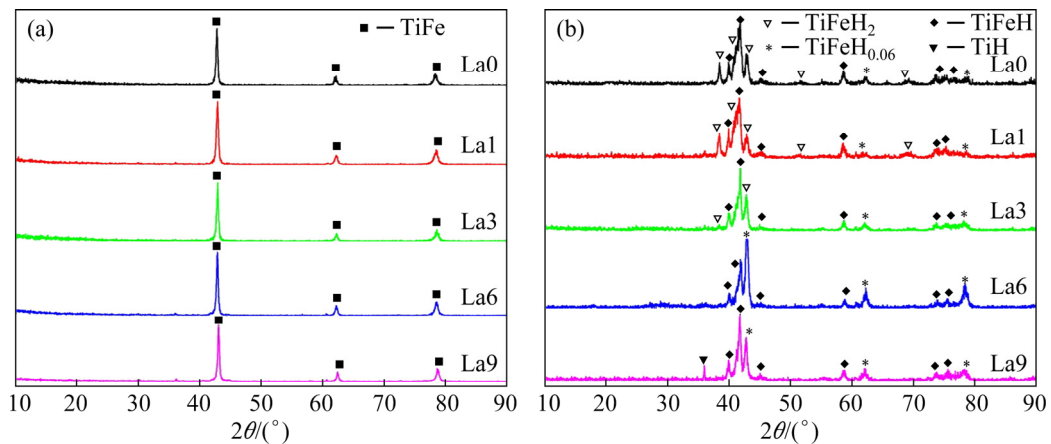


Fig. 1 XRD patterns of as-spun $\text{Ti}_{1-x}\text{La}_x\text{Fe}_{0.8}\text{Mn}_{0.2}$ ($x=0, 0.01, 0.03, 0.06, 0.09$) alloys: (a) Before hydrogenation; (b) After hydrogenation

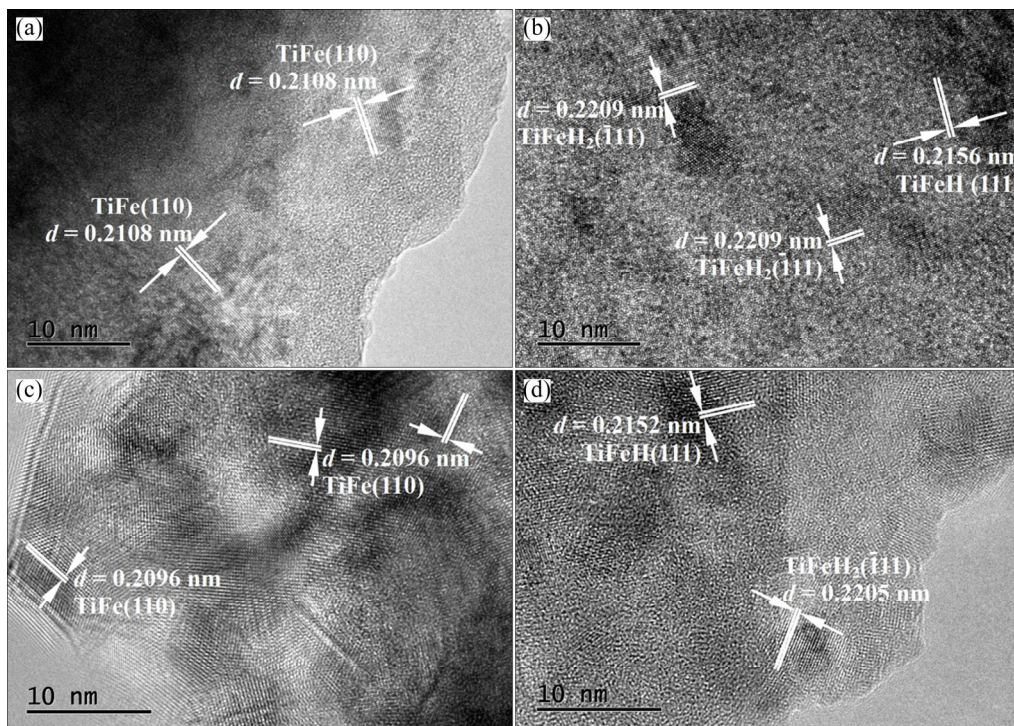


Fig. 2 HRTEM images of La0 before (a) and after (b) hydrogenation, and La1 before (c) and after (d) hydrogenation

TiFeH₂ phases are detected in the alloys after hydrogenation (Figs. 2(b) and (d)). When Ti in the alloy is substituted by La, the spacing of TiFe (110) planes is decreased from 0.2108 to 0.2096 nm. This discovery can be attributed to the larger atomic radius of La than that of Ti. SHANG et al [34] also reported that interplanar crystal spacing becomes narrow after rare earth substitution. Many structural defects such as lattice dislocations and partial amorphous structures can also be observed when La is substituted for Ti alloys. Moreover, the amounts of nanocrystalline and grain boundaries in the La-substituted alloys are higher than those in

non-substituted ones. After hydrogen absorption, TiFeH₂ phase is embedded in TiFeH phase matrix (Fig. 2(d)). The structural defects and nanocrystalline boundaries introduced by La substitution can facilitate hydrogen diffusion [34].

3.2 Hydrogen storage kinetics

Prior to hydrogen absorption kinetics test, all the as-spun alloys were fully activated by three hydrogenation/dehydrogenation cycles under the conditions of 3 MPa and 423 K, and the obtained plots are presented in Fig. 3. The as-spun Ti_{1-x}La_xFe_{0.8}Mn_{0.2} ($x=0, 0.01, 0.03, 0.06, 0.09$)

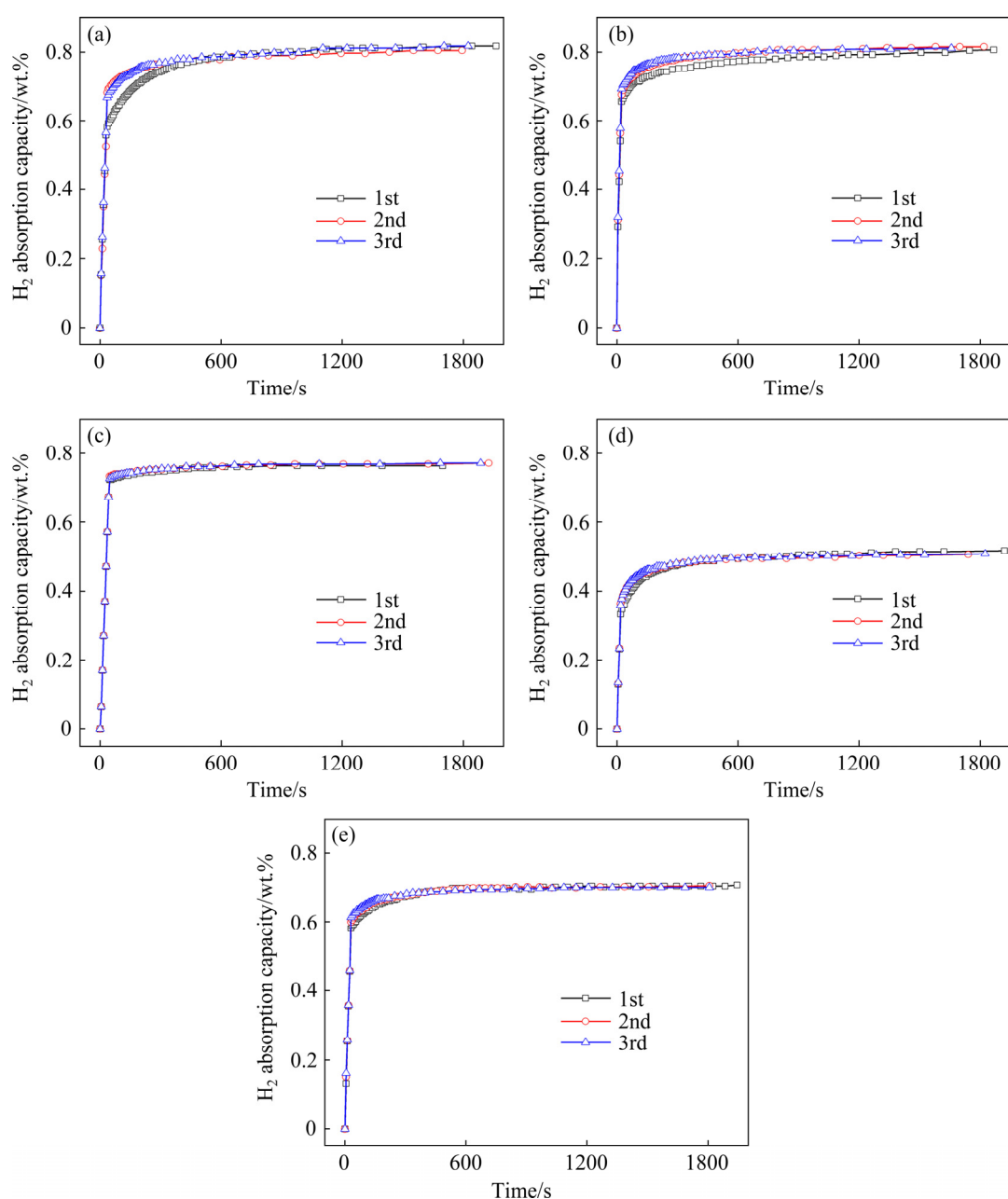


Fig. 3 Hydriding cycle curves of as-spun Ti_{1-x}La_xFe_{0.8}Mn_{0.2} ($x=0, 0.01, 0.03, 0.06, 0.09$) alloys at 3 MPa and 423 K: (a) La0; (b) La1; (c) La3; (d) La6; (e) La9

alloys exhibit good activation ability and can absorb hydrogen in the first cycle. Besides, almost no incubation period is required. Therefore, La substitution reduces the time of hydriding reaction and improves the activation ability of the alloy.

Figure 4 shows the hydrogen absorption kinetic curves of the as-spun alloys at 303, 323, 343, and 363 K. All as-spun alloys have relatively fast absorption kinetics at above temperatures, especially La1 alloy at 303 K. After full activation, all these alloys could absorb hydrogen to saturation within 3 min. The hydrogen absorption capacities of the as-spun alloys are listed in Table 1. The La1 alloy has the maximum hydrogen absorption capacity of (1.80 ± 0.04) wt.% at the temperature of 323 K in all as-spun alloys. The hydrogen storage capacity decreases with increasing La content from 0.01 to 0.06. However, the hydrogen absorption capacity increases when $x=0.09$. This finding can be attributed to the structural characteristic discussed in the XRD and HRTEM analysis. With increasing La content to 0.06, the amount of $\text{TiFeH}_{0.06}$ phase in La6 alloy also increases. Hence, the hydrogen

storage is less than that of TiFeH_2 phase. The TiH hydride phase is also found in the hydrogenated La9 alloy and it has contributed to the increase in the hydrogen capacity.

3.3 Hydrogen storage thermodynamics

The hydrogen absorption/desorption thermodynamic properties of the as-spun $\text{Ti}_{1-x}\text{La}_x\text{Fe}_{0.8}\text{Mn}_{0.2}$ ($x=0, 0.01, 0.03, 0.06, 0.09$) alloys were evaluated by pressure composition isotherms (PCI) curves. The wide range of hydrogen absorption with almost horizontal plateau pressure is important for the application of TiFe type materials. All the alloys have two plateau regions during hydrogen absorption/desorption. The α -TiFe phase changes to TiFeH and TiFeH_2 during hydrogen desorption [30]. Therefore, the two plateau regions represent the two hydrogen absorption/desorption steps in all the alloys. The lower plateaus with the hydrogen capacity ranging from 0 to 1 wt.% correspond to the reversible reaction of TiFe to TiFeH , and the higher plateaus with the hydrogen capacity ranging from 1 wt.% to 1.6 wt.% match the reversible reaction of

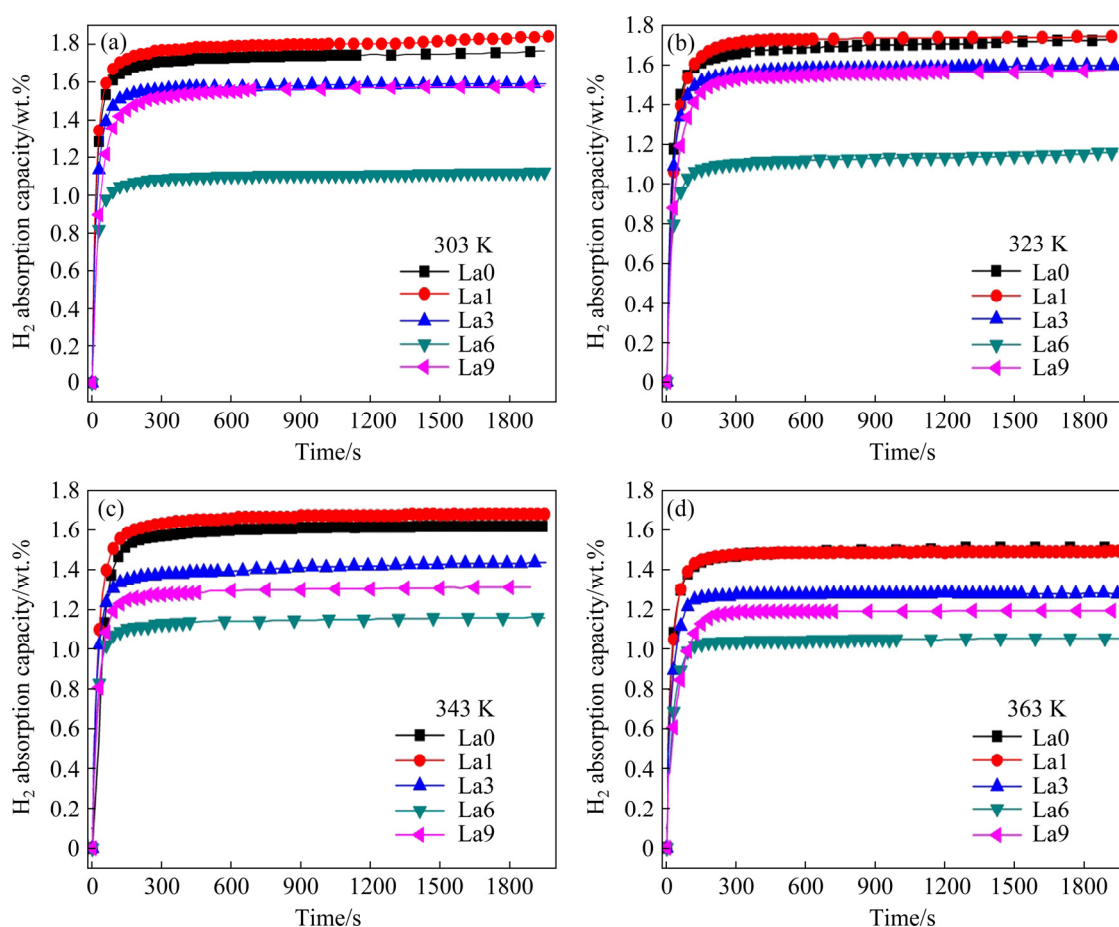


Fig. 4 Hydrogen absorption kinetic curves of as-spun $\text{Ti}_{1-x}\text{La}_x\text{Fe}_{0.8}\text{Mn}_{0.2}$ alloys at different temperatures: (a) 303 K; (b) 323 K; (c) 343 K; (d) 363 K

Table 1 Hydrogen absorption capacities of alloys at different temperature (wt.%)

Alloy	303 K	323 K	343 K	363 K
La0	1.79±0.04	1.75±0.03	1.63±0.03	1.53±0.03
La1	1.76±0.04	1.80±0.04	1.69±0.03	1.50±0.03
La3	1.61±0.03	1.62±0.03	1.44±0.03	1.28±0.03
La6	1.18±0.02	1.20±0.02	1.16±0.02	1.06±0.02
La9	1.67±0.03	1.58±0.03	1.33±0.03	1.20±0.02

TiFeH to TiFeH₂. Figure 5 shows that La substitution substantially influences the equilibrium pressure plateaus in PCI curves. The plateau pressure is heightened, and the plateau width is shortened by increasing La content.

The pressure plateau is closely related to the enthalpy changes of the hydride. Hence, the enthalpy change (ΔH) and entropy change (ΔS) for the hydrogen absorption/desorption of the reversible reaction of TiFe to TiFeH were evaluated by the pressure plateaus at different temperatures. The ΔH and ΔS values can be calculated by the

Van't Hoff plot:

$$\ln(P/P^\ominus) = \Delta H/(RT) - \Delta S/R$$

where P is the equilibrium pressure (MPa). Given that the plateau of TiFe phase is not flat during hydrogenation/dehydrogenation, the plateau pressure is chosen at the median of pressure corresponding to the 20% of the maximum hydrogen absorption capacity. P^\ominus is the standard atmosphere pressure (MPa), R is the gas constant (8.314 J/(K·mol)), and T is temperature (K).

On the basis of the plateau pressures obtained from PCI curves at 303, 323, 343, and 363 K, the ΔH and ΔS values for the hydrogen absorption/desorption can be obtained from the slope and intercept of the Van't Hoff plots, as shown in Fig. 6. The absolute value of hydrogen absorption enthalpy change ($|\Delta H_{ab}|$) firstly increases and then decreases with increasing the La content. When La content is 0.01, the maximum absolute value of enthalpy change is (25.23±0.50) and (30.06±0.60) kJ/mol for the hydrogenation and dehydrogenation, respectively. A low absolute value of ΔH indicates the instability of the hydrides.

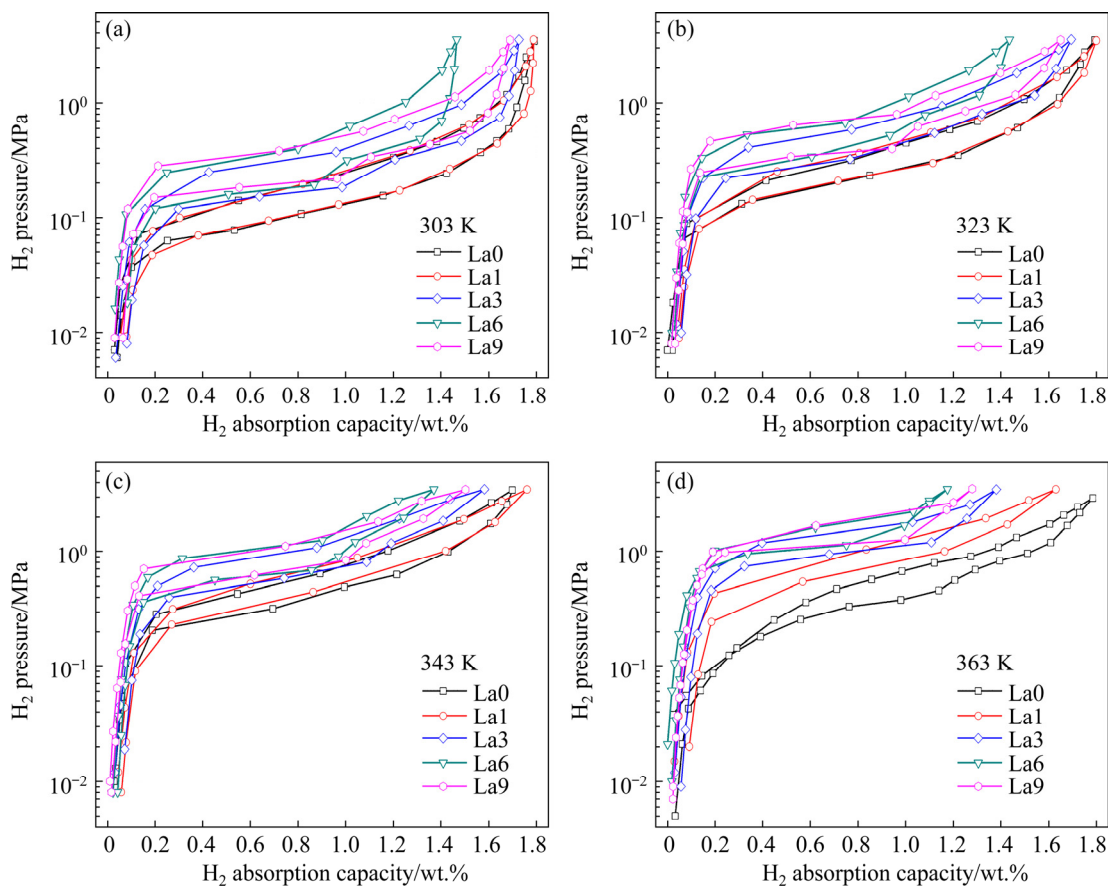


Fig. 5 PCI curves of as-spun Ti_{1-x}La_xFe_{0.8}Mn_{0.2} ($x=0, 0.01, 0.03, 0.06, 0.09$) alloys at different temperatures: (a) 303 K; (b) 323 K; (c) 343 K; (d) 363 K

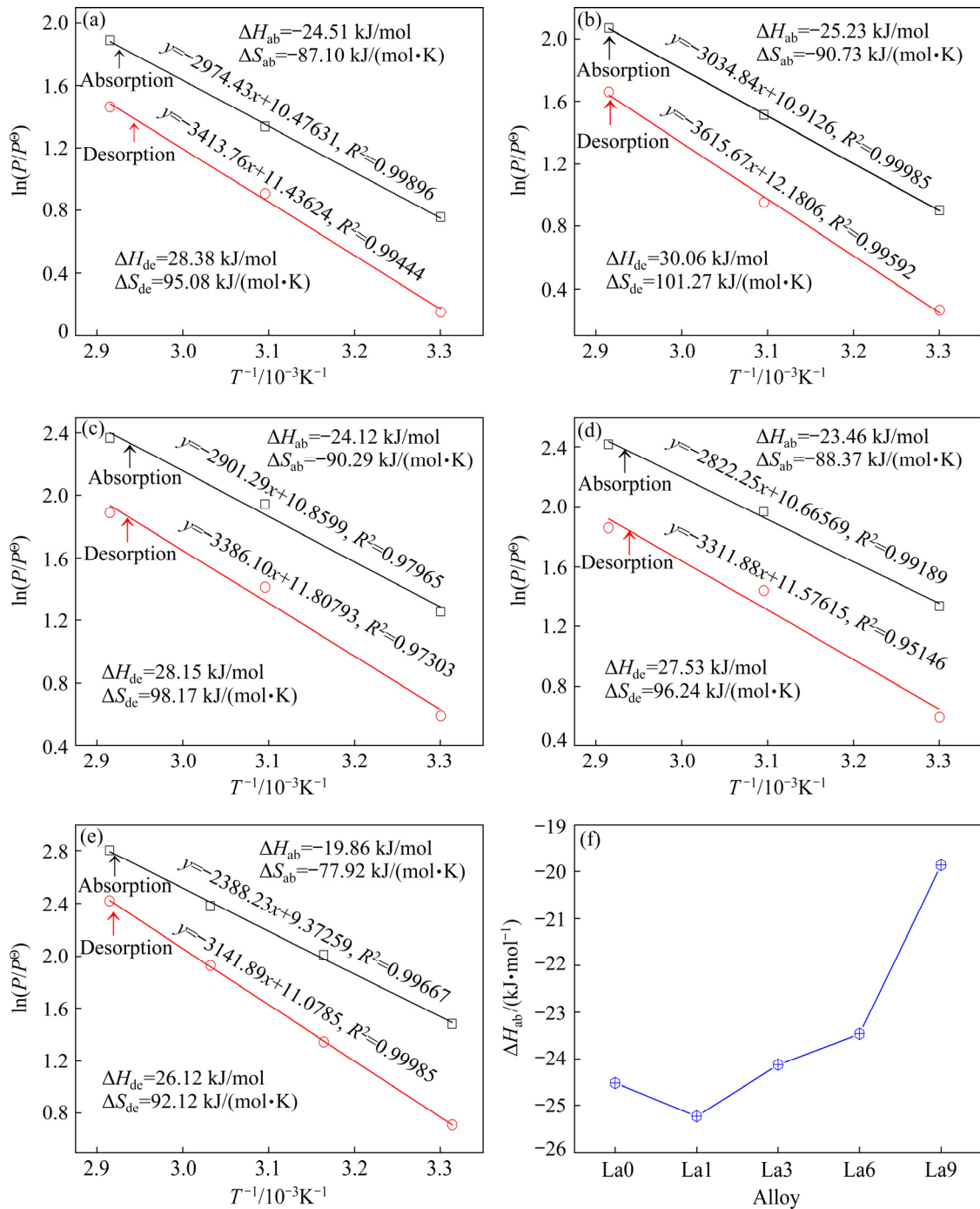


Fig. 6 Van't Hoff plots and enthalpy change of as-spun Ti_{1-x}La_xFe_{0.8}Mn_{0.2} ($x=0, 0.01, 0.03, 0.06, 0.09$) alloys for hydrogen absorption/desorption process at different temperatures: (a) La0; (b) La1; (c) La3; (d) La6; (e) La9; (f) ΔH_{ab}

4 Conclusions

(1) The as-spun Ti_{1-x}La_xFe_{0.8}Mn_{0.2} ($x=0, 0.01, 0.03, 0.06, 0.09$) alloys contain the TiFe phase, indicating that La substitution does not change the phase composition of the alloys. After hydrogen absorption, the TiFeH_{0.06}, TiFeH, and TiFeH₂ phases exist in the alloys. The TiH phase appears when the

La content is 0.09.

(2) The hydrogen storage capacity slightly increases firstly and then decreases with La content varying from 0.01 to 0.09. The La1 alloy holds the maximum hydrogen capacity of (1.80±0.04) wt.% at 323 K.

(3) The plateau pressure is heightened with increasing La content. The absolute value of

hydrogenation enthalpy change $|\Delta H|$ increases firstly and then decreases with increasing La content. The La1 alloy exhibits the maximum absolute value of hydrogenation enthalpy change $|\Delta H|$, implying that hydride of La1 alloy is unstable.

Acknowledgments

The authors are grateful for the financial supports from the Inner Mongolia Natural Science Foundation, China (No. 2019BS05005), the Inner Mongolia University of Science and Technology Innovation Fund, China (No. 2019QDL-B11), and the National Natural Science Foundation of China (Nos. 51901105, 51871125, 51761032).

References

- [1] ZHANG Fang, ZHAO Peng-cheng, NIU Meng, MADDY J. The survey of key technologies in hydrogen energy storage [J]. *International Journal of Hydrogen Energy*, 2016, 41(33): 14535–14552.
- [2] LI Zhen-yang, LI Sheng-li, YUAN Ze-ming, ZHANG Yang-huan, QI Yan. Microstructure, hydrogen storage thermodynamics and kinetics of $\text{La}_5\text{Mg}_{95-x}\text{Ni}_x$ ($x=5, 10, 15$) alloys [J]. *Transactions of Nonferrous Metals Society of China*, 2019, 29(5): 1057–1066.
- [3] WEI T Y, LIM K L, TSENG Y S, CHAN S L I. A review on the characterization of hydrogen in hydrogen storage materials [J]. *Renewable and Sustainable Energy Reviews*, 2017, 79: 1122–1133.
- [4] ZHAN Le-yu, ZHANG Yao, ZHU Yun-feng, ZHUANG Xiang-yang, WAN Neng, QU Yi, GUO Xin-li, CHEN Jian, WANG Zeng-mei, LI Li-quan. Electrochemical performances of $\text{Mg}_{45}\text{M}_5\text{Co}_{50}$ ($\text{M}=\text{Pd}, \text{Zr}$) ternary hydrogen storage electrodes [J]. *Transactions of Nonferrous Metals Society of China*, 2016, 26(5): 1388–1395.
- [5] OUYANG Liu-zhang, HUANG Jian-ling, WANG Hui, LIU Jiang-wen, ZHU Min. Progress of hydrogen storage alloys for Ni–MH rechargeable power batteries in electric vehicles: A review [J]. *Materials Chemistry and Physics*, 2017, 200: 164–178.
- [6] ZHANG X L, LIU Y F, ZHANG X, HU J J, GAO M X, PAN H G. Empowering hydrogen storage performance of MgH_2 by nanoengineering and nanocatalysis [J]. *Materials Today Nano*, 2020, 9: 100064.
- [7] CHEN Yun, CHEN Chang-pin, CESAR S, CHEN Li-xin, WANG Qi-dong. Hydrogen storage properties of Mg-doped $\text{Ti}_{1.2}\text{Fe}$ alloys synthesized by mechanical alloying [J]. *Transactions of Nonferrous Metals Society of China*, 2003, 13(2): 249–253.
- [8] HOSNI B, KHAIDI C, ELKEDIM O, FENINECHE N, LAMLOUMI J. Structure and electrochemical hydrogen storage properties of Ti–Fe–Mn alloys for Ni–MH accumulator application [J]. *Journal of Alloys and Compounds*, 2019, 781: 1159–1168.
- [9] DAVIDS W M, LOTOTSKYY M. Influence of oxygen introduced in TiFe-based hydride forming alloy on its morphology, structural and hydrogen sorption properties [J]. *International Journal of Hydrogen Energy*, 2012, 37(23): 18155–18162.
- [10] ENDO N, SAITOH H, MACHIDA A, KATAYAMA Y. Formation of BCC TiFe hydride under high hydrogen pressure [J]. *International Journal of Hydrogen Energy*, 2013, 38(16): 6726–6729.
- [11] CIRIC K D, KOCJAN A, GRADISEK A, KOTESKI V J, KALIJADIS A M, IVANOVSKI V N, LAUSEVIC Z N, STOJIE D L. A study on crystal structure, bonding and hydriding properties of Ti–Fe–Ni intermetallics-behind addition of iron by nickel [J]. *International Journal of Hydrogen Energy*, 2012, 37(10): 8408–8417.
- [12] ZLATANOVA Z, SPASSOV T, EGGELER G, SPASSOVA M. Synthesis and hydriding/dehydriding properties of $\text{Mg}_2\text{Ni-AB}$ ($\text{AB}=\text{TiNi}$ or TiFe) nanocomposites [J]. *International Journal of Hydrogen Energy*, 2011, 36(13): 7559–7566.
- [13] SCHLAPBACH L, RIESTERER T. The activation of FeTi for hydrogen absorption [J]. *Applied Physics A*, 1983, 32: 169–182.
- [14] LEE J Y, PARK C N, PYUN S M. The activation process and hydriding kinetics of FeTi [J]. *Journal of the Less Common Metals*, 1983, 89(1): 163–168.
- [15] SCHOBER T, WASTLAKE D G. The activation of FeTi for hydrogen storage: A different view [J]. *Scripta Metallurgica*, 1981, 15(8): 913–918.
- [16] JAIN P, GOSSELIN C, HUOT J. Effect of Zr, Ni and $\text{Zr}_7\text{Ni}_{10}$ alloy on hydrogen storage characteristics of TiFe alloy [J]. *International Journal of Hydrogen Energy*, 2015, 40(47): 16921–16927.
- [17] LV P, HUOT J. Hydrogen storage properties of $\text{Ti}_{0.95}\text{FeZr}_{0.05}$, $\text{TiFe}_{0.95}\text{Zr}_{0.05}$ and $\text{TiFeZr}_{0.05}$ alloys [J]. *International Journal of Hydrogen Energy*, 2016, 41(47): 22128–22133.
- [18] LV P, HUOT J. Hydrogenation improvement of TiFe by adding ZrMn_2 [J]. *Energy*, 2017, 138: 375–382.
- [19] MANNA J, TOUGAS B, HUOT J. Mechanical activation of air exposed TiFe + 4 wt.% Zr alloy for hydrogenation by cold rolling and ball milling [J]. *International Journal of Hydrogen Energy*, 2018, 43(45): 20795–20800.
- [20] ABRASHEV B, SPASSOV T, BLIZNAKOV S, POPOV A. Microstructure and electrochemical hydriding/dehydriding properties of ball-milled TiFe-based alloys [J]. *International Journal of Hydrogen Energy*, 2010, 35(12): 6332–6337.
- [21] ZADOROZHNYI V, MILOVZOROV G, KLYAMKIN S, ZADOROZHNYI M, STRUGOVA D, GORSHENKOV M, KALOSHKIN S. Preparation and hydrogen storage properties of nanocrystalline TiFe synthesized by mechanical alloying [J]. *Progress in Natural Science: Materials*, 2017, 27(1): 149–155.
- [22] JANKOWSKA E, JURCZYK M. Electrochemical properties of sealed Ni–MH batteries using nanocrystalline TiFe-type anodes [J]. *Journal of Alloys and Compounds*, 2004, 372(1–2): L9–L12.
- [23] EDALATI K, MATSUDA J, IWAOKA H, TOH S, AKIBA E, HORITA Z. High-pressure torsion of TiFe intermetallics for activation of hydrogen storage at room temperature with

- heterogeneous nanostructure [J]. International Journal of Hydrogen Energy, 2013, 38(11): 4622–4627.
- [24] WILLIAMS M, LOTOTSKYY M V, DAVIDS M W, LINKOV V, YARTYS V A, SOLBERG J K. Chemical surface modification for the improvement of the hydrogenation kinetics and poisoning resistance of TiFe [J]. Journal of Alloys and Compounds, 2011, 509(S2): s770–s774.
- [25] ZALUSKI L, ZALUSKA A, TESSIER P, STRÖM-OLSEN J O, SCHULZ R. Catalytic effect of Pd on hydrogen absorption in mechanically alloyed Mg_2Ni , $LaNi_5$ and FeTi [J]. Journal of Alloys and Compounds, 1995, 217(2): 295–300.
- [26] SHANG Hong-wei, ZHANG Yang-huan, LI Ya-qin, QI Yan, GUO Shi-hai, ZHAO Dong-liang. Effects of adding over-stoichiometrical Ti and substituting Fe with Mn partly on structure and hydrogen storage performances of TiFe alloy [J]. Renewable Energy, 2019, 135: 1481–1498.
- [27] LI Ya-qin, SHANG Hong-wei, ZHANG Yang-huan, LI Ping, QI Yan, ZHAO Dong-liang. Investigations on gaseous hydrogen storage performances and reactivation ability of as-cast $TiFe_{1-x}Ni_x$ ($x=0, 0.1, 0.2$ and 0.4) alloys [J]. International Journal of Hydrogen Energy, 2019, 44(8): 4240–4252.
- [28] SHANG Hong-wei, ZHANG Yang-huan, LI Ya-qin, QI Yan, GUO Shi-hai, ZHAO Dong-liang. Investigation on gaseous and electrochemical hydrogen storage performances of as-cast and milled $Ti_{1.1}Fe_{0.9}Ni_{0.1}$ and $Ti_{1.09}Mg_{0.01}Fe_{0.9}Ni_{0.1}$ alloys [J]. International Journal of Hydrogen Energy, 2018, 43(3): 1691–1701.
- [29] LENG Hai-yan, YU Zhi-gang, YIN Jie, LI Qian, WU Zhu, CHOU Kuo-chih. Effects of Ce on the hydrogen storage properties of $TiFe_{0.9}Mn_{0.1}$ alloy [J]. International Journal of Hydrogen Energy, 2017, 42(37): 23731–23736.
- [30] EMAMI H, EDALATI K, MATSUDA J, AKIBA E, HORITAA Z. Hydrogen storage performance of TiFe after processing by ball milling [J]. Acta Materialia, 2015, 88: 190–195.
- [31] ZEAITER A, CHAPPELLE D, CUEVAS F, MAYNADIER A, LATROCHE M. Milling effect on the microstructural and hydrogenation properties of $TiFe_{0.9}Mn_{0.1}$ alloy [J]. Powder technology, 2018, 339: 903–910.
- [32] WANG Xin-hua, CHEN Ru-gan, CHEN Chang-pin, WANG Qi-dong. Hydrogen storage properties of $Ti_xFe + ywt.\%La$ and its use in metal hydride hydrogen compressor [J]. Journal of Alloy and Compounds, 2006, 425: 291–295.
- [33] YANG Tai, WANG Peng, XIA Chao-qun, LIU Ning, LIANG Chun-yong, YIN Fu-xing, LI Qiang. Effect of chromium, manganese and yttrium on microstructure and hydrogen storage properties of TiFe-based alloy [J]. International Journal of Hydrogen Energy, 2020, 45(21): 12071–12081.
- [34] SHANG Hong-wei, LI Ya-qin, ZHANG Yang-huan, QI Yan, GUO Shi-hai, ZHAO Dong-liang. Structure and hydrogenation performances of as-cast $Ti_{1.1-x}RE_xFe_{0.8}Mn_{0.2}$ ($RE=Pr, Sm$ and Nd ; $x=0, 0.01$) alloys [J]. International Journal of Hydrogen Energy, 2018, 43(41): 19091–19101.

La 替代对快淬 Ti–Fe–Mn 基合金显微组织和贮氢性能的影响

袁泽明^{1,2}, 祁震^{1,2}, 翟亭亭¹, 王鸿章¹, 王海燕¹, 张羊换^{1,2}

1. 内蒙古科技大学 分析测试中心, 包头 014010;
2. 钢铁研究总院 功能材料研究所, 北京 100081

摘要: 采用熔融纺丝法制备 $Ti_{1-x}La_xFe_{0.8}Mn_{0.2}$ ($x=0, 0.01, 0.03, 0.06, 0.09$, 摩尔分数)快淬态合金。研究 La 替代 Ti 对 TiFe 型 Ti–Fe–Mn 基合金显微组织、贮氢动力学和贮氢热力学的影响。所有快淬态合金均保持单一的 TiFe 相; 加氢后, TiFe 相转变为 $TiFeH_{0.06}$ 、TiFeH 和 $TiFeH_2$ 氢化物。La 替代促进合金微观缺陷(如位错和晶界)的产生, 这利于氢扩散。此外, La 替代还提高储氢动力学性能。随 La 含量的增加, 合金的贮氢容量先减小后增大, 氢化焓变的绝对值($|\Delta H|$)先增大后减小。当 $x=0.01$ 时, 合金加氢焓变的绝对值 $|\Delta H|$ 最大, 为 (25.23 ± 0.50) kJ/mol, 在 323 K、3 MPa 条件下合金的最大贮氢容量为 (1.80 ± 0.04) wt.%。

关键词: La 替代; Ti–Fe–Mn 基合金; 熔融纺丝; 贮氢动力学; 热力学

(Edited by Wei-ping CHEN)